Modeling of Bilayer Hydrogel Springs for Microrobots with Adaptive Locomotion

Liyuan Tan and David J. Cappelleri

Abstract—Adaptive locomotion of microrobots can be achieved by using a smart polymer such as a hydrogel. For hydrogel-based bilayer helical microrobots, the change of environment such as temperature and pH can result in shape deformation into helical shapes differing from their initial state and hence swimming performance. In this work, we proposed a model for studying the parameters that affect the shape deformation of a hydrogel-based bilayer helical microrobot. Moreover, the dynamics of some examples of responsive helical swimming are compared before and after stimulation.

I. INTRODUCTION

Smart polymers have been widely investigated in the past decade achieving shape transformation of structures exhibiting mean and Gaussian curvatures [1], [2]. Structures that are made of smart polymers are able to change their shapes under certain environmental stimuli such as temperature, pH, and chemicals, after fabrication. Typical smart polymers are hydrogels and liquid crystalline polymers. Pure hydrogels generally perform isotropic transformation and liquid crystalline polymers transform anisotropically [3].

In the microrobotic domain, bilayer structures, typically consisting of a responsive layer and a non-responsive layer, been used to fabricate microgrippers micromanipulation and helical microrobots for adaptive locomotion [4], [5]. The microgrippers are typically controlled by a gradient magnetic field because they do not have an advanced component for locomotion [6]. The latter helical microrobots are usually actuated using a rotating magnetic field and achieve more significant for translation capabilities [5]. These types of smart polymer-based helical microrobots are able to adjust their shapes under different environmental stimuli, resulting in a variation of their swimming dynamics. Moreover, a microrobot with adaptive locomotion can accommodate different sized microfluidic environments such as blood vessels with different diameters for bio-applications.

Recently, the development of direct laser writing (DLW) introduced more design freedom of microrobots and simplicity when compared with those fabricated by traditional microfabrication techniques such as photolithography when the initial state of the structure is limited to be two-dimensional. Also, a helical structure can only be achieved when anisotropy is introduced to the structure [3]. Microrobots made from both non-responsive and responsive materials have been fabricated in the past few years by DLW

This work was supported by the National Science Foundation (NSF IIS Award 1763689).

Liyuan Tan is with the School of Mechanical Engineering, Purdue University, West Lafayette, IN 47907, USA. tan328@purdue.edu

David J. Cappelleri is with the Faculty of Mechanical Engineering, Purdue University, West Lafayette, IN 47907, USA. dcappell@purdue.edu [7], [8]. However, a responsive swimming helical type microrobot has not been achieved with DLW yet.

The dynamics of microrobots have also been investigated in the past few years including helical type microrobots and microrobots with arbitrary shapes. The dynamics of the former one has been studied by different methods [9], [10] while the latter one has only been studied by Morozov et al. [11]. These theories have been applied to rigid or flexible microrobots; however, they are not used to study the dynamics transformation of a responsive swimming helical type microrobots.

In this work, we propose a finite element model to study the temperature-induced shape transformation of a bilayer helical spring fabricated through DLW with hydrogel material as a design tool to create an adaptive helical swimming microrobot. The finite element model is built in ABAQUS [12] with a UHYPER subroutine [13] to define the swelling or shrinking of the hydrogel material. The discontinuous change of the volume ratio that introduces sudden change of shapes was eliminated by an expansion series which allows the investigation of continuous shape deformation over the entire temperature domain of interest. Last, the dynamics transformation of some responsive swimming helical type microrobots are investigated for the dynamics change before and after the stimulation.

II. METHOD

A. Free Energy Model for Hydrogels

The constitutive model of a hydrogel can be represented by the Helmholtz free energy when the crosslinking density is assumed to have little effects on the interaction between the monomers and the solvent molecules. Following the formulation proposed by Cai and Suo [14], the Helmholtz free energy is contributed by two independent parts: (i) the stretching of the network and (ii) the mixing of the polymer and the solvent. Therefore, the Helmholtz free energy is

$$W = W_{stretch} + W_{mix} , \qquad (1)$$

where $W_{stretch}$ is the free energy introduced by the stretching of the network and W_{mix} is the free energy caused by the mixing of the polymer and the solvent.

The free energy caused by stretching of the polymer network can be expressed by [15]

$$W_{stretch} = \frac{1}{2} NkT [F_{ik} F_{ik} - 3 - 2\log(\det \mathbf{F})].$$
 (2)

The energy due to the mixing of monomers and solvents is taken to be [16], [17]

$$W_{mix} = kT \left[C \log \frac{vC}{1 + vC} + \frac{\chi C}{1 + vC} \right], \tag{3}$$

where N is the number of polymer chains per unit dry volume, k is the Boltzmann constant, T is the absolute temperature, v is the volume of per solvent molecule, \mathbf{F} is the deformation gradient corresponding to the network at the dry state, C is the nominal concentration of solvent molecules, and χ is the dimensionless Flory-Huggins parameter characterizing strength of interactions between different species. The $F_{lk}F_{lk}$ here in the dummy notation is the trace of the right Cauchy-Green deformation $\mathbf{C} = \mathbf{F}^T\mathbf{F}$ and is denoted by \overline{I}_1 in the following equations. Following Huggins' result, the χ for a specific hydrogel can be obtained by fitting experimental data in the form below [18]

$$\chi = \chi_0 + \chi_1 \phi \,, \tag{4}$$

where

$$\chi_0 = A_0 + B_0 T$$
 and $\chi_1 = A_1 + B_1 T$, (5)

with

$$\phi = \frac{1}{1 + vC},\tag{6}$$

where ϕ is the volume fraction of the polymer in the hydrogel. A_0 , B_0 , A_1 , and B_1 are fit experimentally and depend on different kinds of hydrogels.

The chemical potential, which is a constant at an equilibrium state, can be introduced as an independent parameter through a Legendre transform of the free energy. The new free energy function can be expressed as

$$\hat{W} = W - \mu C, \tag{7}$$

where μ is the chemical potential.

Assuming that the swelling or shrinking process is only induced by the increasing or decreasing of number of solvent molecules inside the hydrogel (e.g., the hydrogel molecules are incompressible), the following relation can be used [19].

$$J = \det \mathbf{F} = 1 + vC \,, \tag{8}$$

where J is the volume ratio relative to the dry state of the hydrogel.

Combining the above equations, the free energy function \hat{W} has the form:

$$\hat{W} = \frac{1}{2} NkT \left[J^{\frac{2}{3}} \overline{I_1} - 3 - 2\log(J) \right] + \frac{kT}{v} (J - 1) \left[\log\left(\frac{J - 1}{J}\right) + \frac{\chi_0}{J} + \frac{\chi_1}{J^2} \right] - \frac{\mu}{v} (J - 1) \right], \quad (9)$$

At the transition temperature, a sharp change in volume ratio is observed for a temperature-sensitive hydrogel because of a jump of the minimal energy. This phenomenon is disastrous for finite element analysis of continuous deformation hydrogel crossing the transition temperature. This sharp change can be eliminated by using expansion series of the logarithmic term [20].

$$\log\left(\frac{J-1}{J}\right) = -\frac{1}{J} - \frac{1}{2J^2} - \frac{1}{3J^3} - \dots$$
 (10)

The first three terms of the expansion series are chosen both considering the accuracy and the elimination of the sharp change in volume ratio. Therefore, the free energy function becomes

$$\hat{W} = \frac{1}{2} NkT \left[J^{\frac{2}{3}} \overline{I_1} - 3 - 2\log(J) \right] + \frac{kT}{v} (J - 1) \left[-\frac{1}{J} - \frac{1}{2J^2} - \frac{1}{3J^3} + \frac{\chi_0}{J} + \frac{\chi_1}{J^2} \right].$$
(11)
$$-\frac{\mu}{v} (J - 1)$$

This expansion also eliminates the singularity when J=1, where the hydrogel is at its dry state. However, a hydrogel structure is typically not at its dry state after polymerization. A reference state can be adopted for the designed structure before performing any deformation.

The deformation gradient for a free swelling state relative to the dry state is

$$\mathbf{F}_0 = \begin{bmatrix} \lambda_0 & 0 & 0 \\ 0 & \lambda_0 & 0 \\ 0 & 0 & \lambda_0 \end{bmatrix},\tag{12}$$

where λ_0 is the stretch ratio and $J = \lambda_0^3$ for free swelling.

Then the deformation gradient and volume ratio for the current state relative to the dry state can be expressed by

$$\mathbf{F} = \mathbf{F}'\mathbf{F}_0, \tag{13}$$

and

$$J = \lambda_0^3 J' \,. \tag{14}$$

where \mathbf{F}' and J' are deformation gradient and volume ratio for the current state relative to the reference state.

Therefore, the free energy function can be rewritten (8) relative to the reference state

$$\hat{W} = \lambda_0^{-3} \left\{ \frac{1}{2} NkT \left[\lambda_0^2 J^{\frac{2}{3}} \overline{I}_1 - 3 - 2 \log \left(\lambda_0^3 J' \right) \right] + \frac{kT}{\nu} \left(\lambda_0^3 J' - 1 \right) \left[-\frac{1}{\lambda_0^3 J'} - \frac{1}{2\lambda_0^6 J'^2} - \frac{1}{3\lambda_0^9 J'^3} \right] + \frac{\chi_0}{\lambda_0^3 J'} + \frac{\chi_1}{\lambda_0^6 J'^2} \left[-\frac{\mu}{\nu} \left(\lambda_0^3 J' - 1 \right) \right].$$
(15)

Scaling the free energy function by kT/v, we will obtain the final form of the function used for the implementation of the finite element analysis.

With Nv together becomes a dimensionless parameter characterizing the polymer chain density in the dry state, the final form of the free energy function is

$$\hat{W} = \lambda_0^{-3} \left\{ \frac{1}{2} N \nu \left[\lambda_0^2 J^{'\frac{2}{3}} \overline{I}_1 - 3 - 2 \log \left(\lambda_0^3 J' \right) \right] + \left(\lambda_0^3 J' - 1 \right) \left[-\frac{1}{\lambda_0^3 J'} - \frac{1}{2\lambda_0^6 J'^2} - \frac{1}{3\lambda_0^9 J'^3} \right],$$

$$+ \frac{\chi_0}{\lambda_0^3 J'} + \frac{\chi_1}{\lambda_0^6 J'^2} - \frac{\mu}{kT} \left(\lambda_0^3 J' - 1 \right) \right\}$$
(16)

B. Dynamic Model of an Arbitrary-shaped Microrobot

In this work, the helical type microrobots are actuated by rotating magnetic field. The dynamics of an arbitrary-shaped microrobot have been studied by Morozov et al. [11] with details. In brief, the dynamics is described by two coordinate systems. Assuming the microrobot has a permanent magnetic moment:

$$\boldsymbol{H}^{LCS} = H\left(\cos\omega t, \sin\omega t, 0\right),\tag{17}$$

where H and ω are the amplitude and the angular velocity of the rotating magnetic field with the field defined as above in the laboratory coordinate system (LCS).

The second coordinate is the body coordinate system (BCS) fixed to the microrobot. It is used to defines the magnetic moment:

$$\mathbf{m}^{\text{BCS}} = m(n_1, n_2, n_3),$$
 (18)

where m is the magnitude of the magnetic moment and n_i are the projections of the unit vector of the moment. The unit vector $\mathbf{n} = \mathbf{m} / m = n \left(\sin \Phi \cos \alpha, \sin \Phi \sin \alpha, \cos \Phi \right)$ is defined in the BCS in a spherical form where Φ and α are the polar and azimuthal angles.

The two coordinate systems are related by a rotation matrix **R** which is represented by Euler angles φ , ψ , and θ . Therefore, the rotating magnetic field defined in the LCS can be expressed in the BCS by $\boldsymbol{H}^{BCS} = \mathbf{R} \cdot \boldsymbol{H}^{LCS}$.

The dynamics of the swimming microrobot is characterized by the force and torque balances, which are

$$\boldsymbol{U} = \boldsymbol{\mathcal{G}} \cdot \boldsymbol{L}_{m}, \tag{19}$$

$$\mathbf{\Omega} = \mathbf{F} \cdot \mathbf{L}_{m}, \tag{20}$$

where U and Ω are the translational and angular velocities of the microrobot, and \mathcal{G} and \mathcal{F} are the coupling and rotation mobility tensors of the microrobot that only depend on the geometry of the microrobot. In the synchronous regime, the microrobot is rotating with the rotating magnetic field at the same angular frequency and direction while having a phase difference which results in the magnetic torque $L_m = m \times H$. The coupling and rotation mobility tensors can be obtained by the multipole expansion method by approximating the microrobot by spheres [21].

Therefore, the dynamics can be obtained by solving (20) first. The equations can be reduced and readily provided by [11].

$$\frac{1+\varepsilon}{\omega_0} \left(\dot{\varphi} s_{\theta} s_{\psi} + \dot{\theta} c_{\psi} \right) = n_2 s_{\theta} s_{\tilde{\varphi}} + n_3 \left(c_{\tilde{\varphi}} s_{\psi} + s_{\tilde{\varphi}} c_{\psi} c_{\theta} \right), \quad (21)$$

$$\frac{1-\varepsilon}{\omega_0} \left(\dot{\varphi} s_\theta c_\psi - \dot{\theta} s_\psi \right) = -n_3 s_\theta s_{\tilde{\varphi}} + n_3 \left(c_{\tilde{\varphi}} c_\psi - s_{\tilde{\varphi}} s_\psi c_\theta \right), \quad (22)$$

$$\frac{1}{p\omega_0} (\dot{\varphi} c_\theta + \dot{\psi}) = -n_\perp \left(c_{\tilde{\varphi}} s_{\psi+\alpha} + s_{\tilde{\varphi}} c_{\psi+\alpha} c_\theta \right), \tag{23}$$

where $\tilde{\varphi} = \varphi - \omega t$ and $n_{\perp} = \sin \Phi$. The ω_0 is the characteristic frequency and $\omega_0 = mH\mathcal{F}_{\perp}$ where $\mathcal{F}_{\perp}^{-1} = \left(\mathcal{F}_1^{-1} + \mathcal{F}_2^{-1}\right)/2$, $p = \mathcal{F}_3 / \mathcal{F}_{\perp}$, and $\varepsilon = \left(\mathcal{F}_2 - \mathcal{F}_1\right)/\left(\mathcal{F}_2 + \mathcal{F}_1\right)$. For synchronous states, the Euler angles φ , ψ , and θ are independent of time and are constants. The translational velocity can be then calculated from (19).

C. Magnetic Moment of Helical Type Microrobots

Since we assumed that the magnetic properties of the hydrogel microrobots are rendered by the randomly doped magnetic nanoparticles, the direction of the magnetic moment is going to change for different shapes of microrobots. This is called shape-controlled magnetic moment (with an easy axis for magnetization). The direction of the magnetic moment of a helical microrobot have been studied in [22], [23]. The calculation of the direction of the magnetic moment are detailed by these references.

The centerline and the basis at each position of a helical microrobot can be parameterized by the arc length, s, according to [23], [24].

$$X(s) = \left[\frac{\kappa}{\lambda^2}\cos(\lambda s), \frac{\kappa}{\lambda^2}\sin(\lambda s), \frac{\tau}{\lambda}s\right],\tag{24}$$

and

$$d_{1}(s) = \left[\frac{\tau}{\lambda}\sin(\lambda s), -\frac{\tau}{\lambda}\cos(\lambda s), \frac{\kappa}{\lambda}\right],$$

$$d_{2}(s) = \left[\cos(\lambda s), \sin(\lambda s), 0\right],$$

$$d_{3}(s) = \left[-\frac{\kappa}{\lambda}\sin(\lambda s), \frac{\kappa}{\lambda}\cos(\lambda s), \frac{\tau}{\lambda}\right],$$
(25)

where s is the arc length, λ , κ , and τ are defined as $\lambda = 1/\sqrt{R^2 + P^2/\left(4\pi^2\right)}$, $\kappa = R\lambda^2$, and $\tau = P\lambda^2/\left(2\pi\right)$, respectively, through helix radius R and pitch P.

Then, the effective susceptibility χ of the helical microrobot can be calculated by

$$\chi = L^{-1} \int_{0}^{L} (\chi_{1} d_{1} d_{1} + \chi_{2} d_{2} d_{2} + \chi_{3} d_{3} d_{3}) ds, \qquad (26)$$

where χ_1 , χ_2 , and χ_3 are eigenvalues and can be obtained by

$$\chi_1 = \frac{\chi_0}{1 + 4\pi\gamma_0 N_1}, \quad \chi_2 = \frac{\chi_0}{1 + 4\pi\gamma_0 N_2}, \quad \chi_3 = \chi_0,$$
(27)

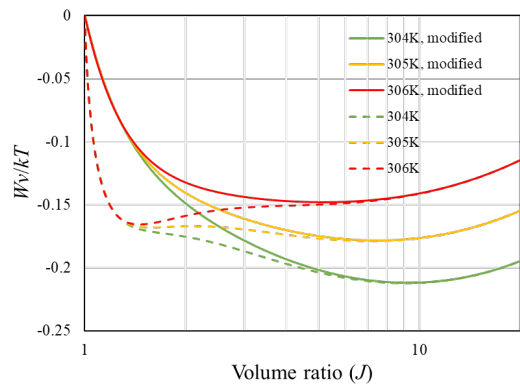


Fig. 1. Analytic solutions of free energy of hydrogel at different temperatures around the transition temperature. The solid lines are energies calculated using the free energy function modified by expansion series. The dash lines are obtained from the standard free energy function without expansion.

with N_1 and N_2 being the demagnetizing factors along d_1 and d_2 .

Finally, the polar angle Φ and azimuthal angle α for the magnetic moment can be calculated by the following relations [23]:

$$\Phi = \cos^{-1}(\hat{\mathbf{v}}_1 \cdot \hat{\mathbf{e}}_3), \quad \cos \alpha = \hat{\mathbf{m}} \cdot \hat{\mathbf{v}}_2, \tag{28}$$

where \hat{v}_1 , \hat{v}_2 are the eigenvectors corresponding to the largest and the second largest eigenvalue of χ , and \hat{e}_3 is the helical axis of the microrobot; \hat{m} is the easy axis of the magnetization which is the unit normal to the plane formed by \hat{v}_1 and \hat{e}_3 .

III. RESULTS AND DISCUSSION

In the following simulations, the dimensionless parameter Nv is set to be 0.01 for a typical hydrogel [25], [26]. The normalized chemical potential μ/kT is 0 for water. In this work, only deformation stimulated by temperature change is investigated; however, the deformation caused by the change of solvents can also be simulated by varying the chemical potential. The hydrogel we adopted in this work is a typical temperature-sensitive hydrogel: poly (N-isopropylacrylamide) (PNIPAM) with material parameters readily provided by Afroze et al. [27]. The fitted parameters are taken as $A_0 = -12.947$, $B_0 = 0.0449 \text{K}^{-1}$, $A_1 = 17.92$, and $B_1 = -0.0569 \text{K}^{-1}$. This

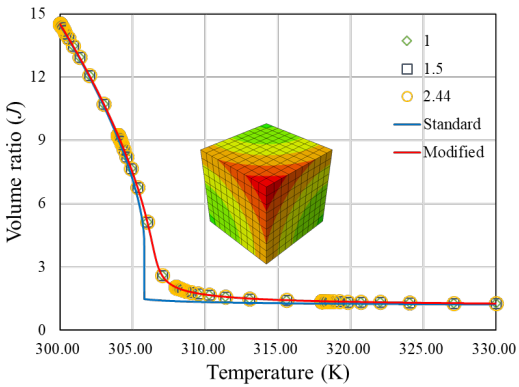


Fig. 2. Change of volume ratio at different temperature of a free swelling cubic block. The volume ratio is calculated through finite element analysis and analytically. 1, 1.5, and 2.44 in the legend are the initial swelling ratio, λ_0 .

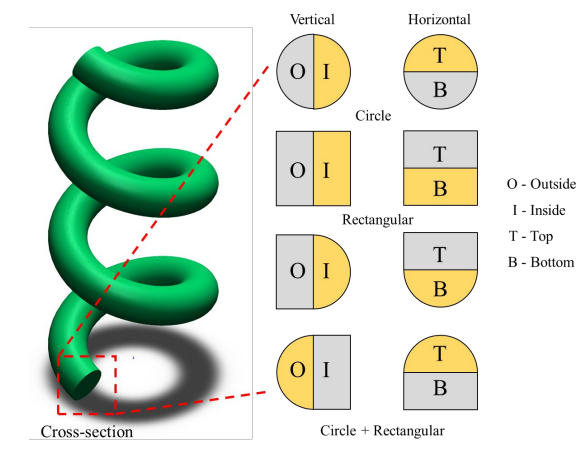


Fig. 3. Illustration of different designed cross-sections of a bilayer helical microrobot. The gray and yellow areas can be either responsive or non-responsive material.

hydrogel is used as the responsive layer in the bilayer helical microrobot while the non-responsive layer is modeled by the classical neo-Hookean hyperelastic model. The magnetic properties that allow the helical microrobots to be actuated by a rotating magnetic field is assumed to be introduced by randomly distributed magnetic nanoparticles that are monodispersed. With this assumption, the isotropy of the hydrogel still holds for the simulation.

A. Smoothing of the Free Energy Function

The swelling ratio of a hydrogel structure is characterized by the free energy function and is stable when the energy is at its local minimum. Fig. 1 provides analytical solutions of the free energy function at different volume ratios and temperatures around the transition temperature. As can be seen from the figure, two local minimum can be observed at 305K using the free energy function that is not modified by the expansion series. At the transition temperature, two local minimums with different volume ratios but identical energy can be expected, which results in a sharp change of volume when the temperature shifts across the transition temperature. With the expansion series, only one local minimum can be found in the whole range of volume ratio with the local minimum at the lower volume ratio eliminated. The expansion only introduces a limited degree of inaccuracy around the transition temperature which is shown later.

B. Validation of the UHYPER Subroutine

The user-defined UHYPER subroutine is validated by comparing the volume ratio of a free swelling cubic block obtained through finite element analysis with the analytical solution. As can be seen in Fig. 2, the subroutine is tested for different initial stretch ratios λ_0 . Swelling from the dry state is characterized by λ_0 = 1 while λ_0 = 2.44 is used for deswelling from 300K. An initial stretch ratio of λ_0 = 1.5 is used for the state after polymerization without loss of generality since different synthesis conditions will result in different initial swelling ratios, λ_0 [26]. Both the volume ratio obtained by the standard and the modified free energy functions are tested. As shown in Fig. 2, a significant discrepancy can only be found around the transition temperature.

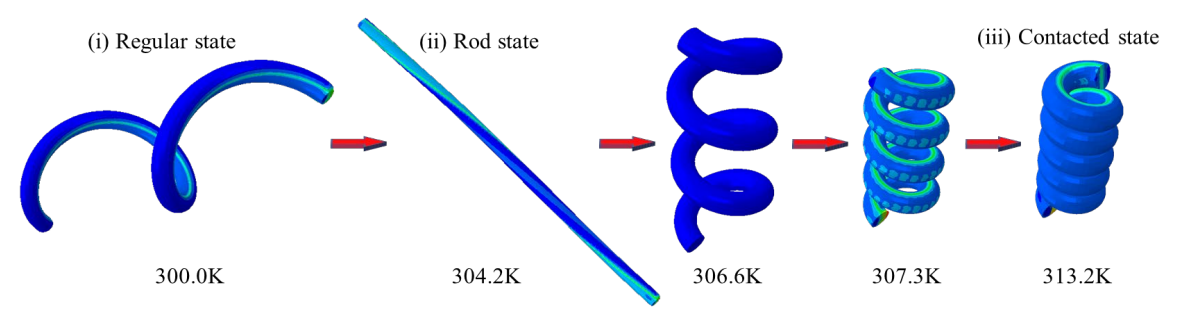


Fig. 4. A shape deformation induced by temperature change. The example microrobot shown has an initial pitch of $100 \mu m$, a circular cross-section, and a inside-located hydrogel.

C. Transformation of Helical Bilayer Microrobots

In this section, the transformations of helical bilayer microrobots are studied with different parameters, i.e., helix pitches, cross-sections, and material arrangements. The initial helix turns of the helical microrobots throughout this work is set to be 3; the transformation of a helix with different number

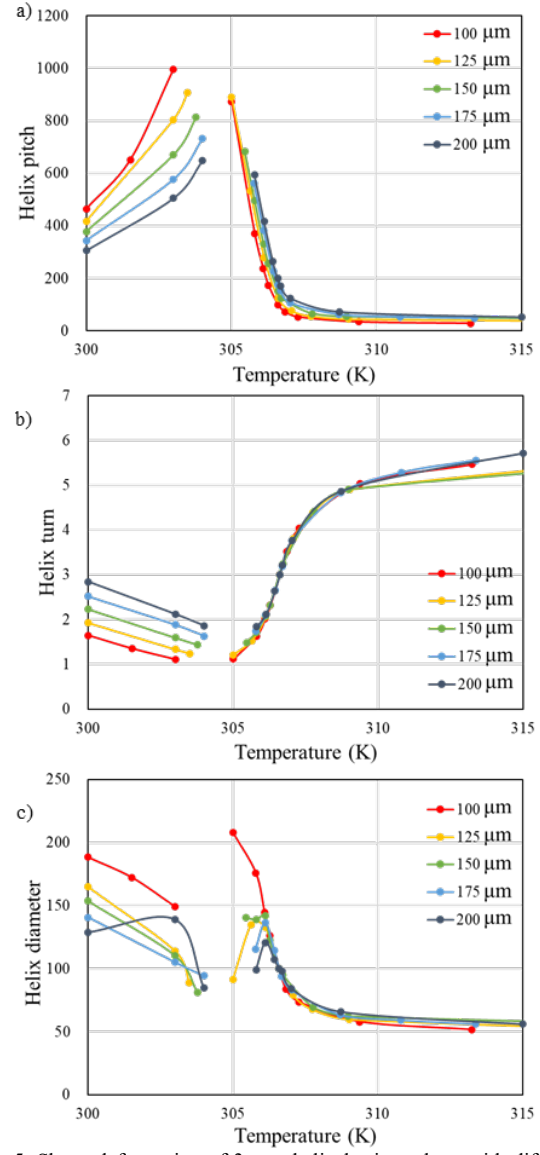


Fig. 5. Shape deformation of 3-turn helical microrobots with different initial helix pitches ranging from initial values of 100 μm to 200 μm.

of turns are proportional as long as the end-effects are negligible. A sketch of a helical microrobot and different cross-sectional designs can be found in Fig. 3. The gray and yellow areas can be either the responsive hydrogel or the non-responsive material; the switching of these two materials leading to different deformations. The shapes of the cross-sections are circular, rectangular, and the combination of them. The arrangement of materials is recognized by the separating boundary of the two materials. A vertical arrangement means that the boundary is vertical while a horizontal arrangement has a horizontal boundary. The positions of different materials are labeled by outside and inside for a vertical arrangement and top and bottom for a horizontal arrangement. The visualizable deformation of a helical bilayer microrobot with pitch of 100 µm and circular cross-section with the responsive hydrogel located at the outside of the helical microrobot is provided in Fig. 4. Three typical states can be observed: (i) regular helical state with non-contacted filament; (ii) rod state with an infinite helix pitch where the helical bilayer is flipped inside out; (iii) contacted state with filament is compacted. The shape deformation data in this section including helix pitch, helix turns, and helix diameter are estimated from the structures calculated by finite element analysis. All models are obtained with an initial temperature of 306.6K which corresponding to an initial swelling ratio of $\lambda_0 = 1.5$. The temperature range presented in the shape deformation is from 300K to 315K, which are temperatures close to the room temperature and temperature where the volume ratio only further changes a little, respectively.

The effects on shape deformation induced by temperature variation are investigated by different helix pitches. As can be seen in Fig. 5, the helical shape for all helix pitches is discontinuous. A rod state can be found at around 305K. This rod state temperature (RST) increases with helix pitch inferred from the figure. The rod state presents a twisted arrangement of the two materials. As depicted in Fig. 5 a), a microrobot with smaller initial helix pitch presents larger helix pitches at temperature below the RST. While for higher temperatures than the RST, the resulting helix pitch increases slightly with different initial pitches. From Fig. 5 b), one can infer that the "turns" of the rod state increases with pitches. The resulting helix turns for different initial pitch values are identical and decrease with temperatures reaching the rod state at different temperatures. After the rod state, the variation is reversed and higher initial pitch results in more turns. The change of helix diameter is more interesting with non-monotonic relationships occurring on both sides of the rod state. Generally, the

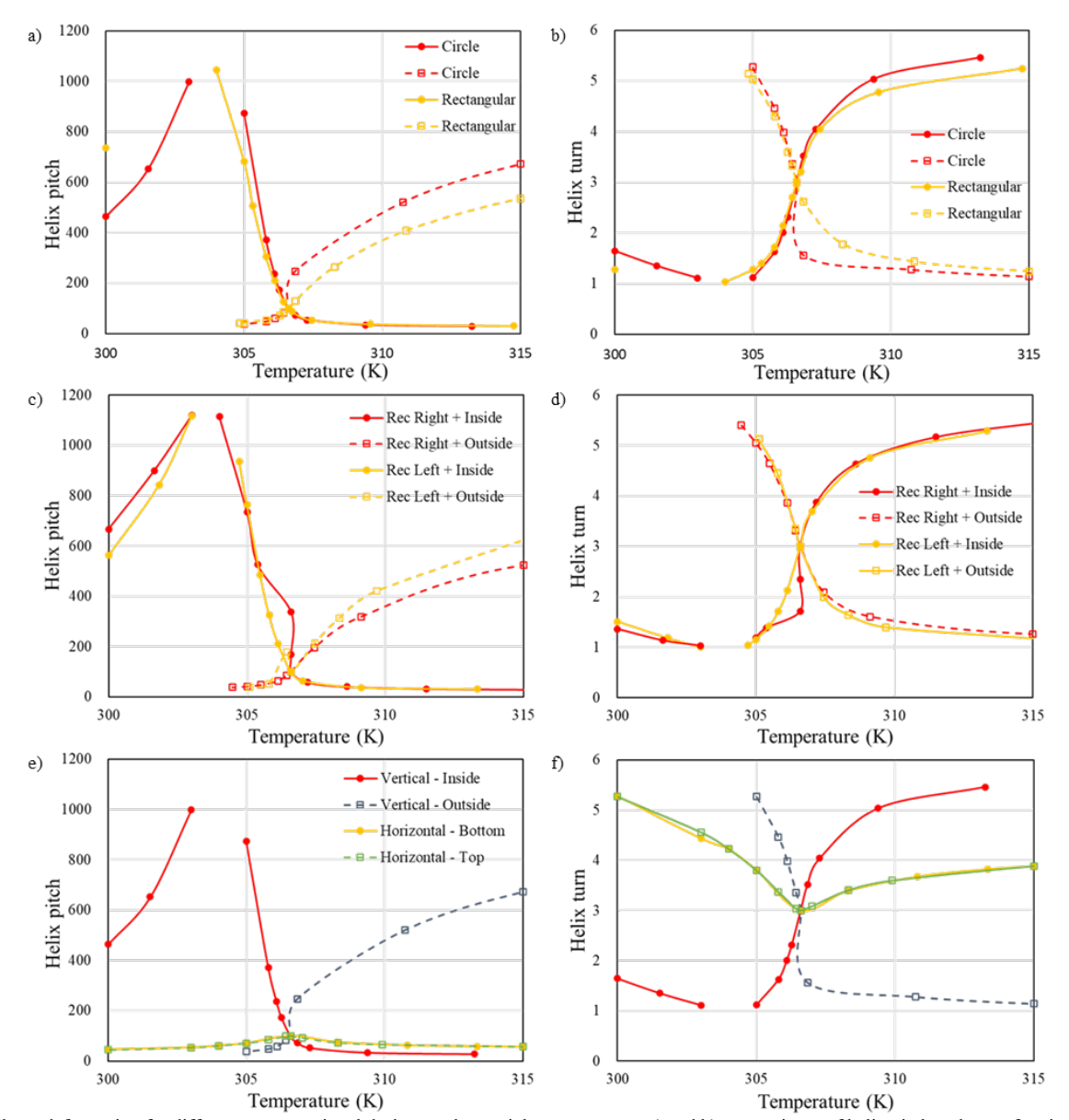
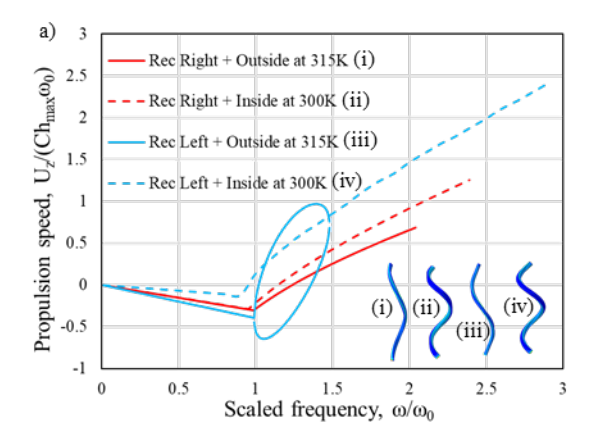


Fig. 6. Shape deformation for different cross-sectional designs and material arrangements. a) and b) comparisons of helix pitch and turns for circular and rectangular cross-sections. Solid lines for material alignments with responsive materials as the outside part while dash lines are for when the responsive material is the inside part. c) and d) Shape deformation data for cross-sections consisting of half circle and rectangular shapes. "Rec" in the legend is represents rectangular. e) and f) Comparisons of shape deformations with vertical and horizontal arrangements. "Inside" and "Outside" in the legend represent the position of the responsive hydrogel.

diameter at a temperature lower than RST increases as temperature decreases; it also decreases with the initial pitch value. At temperatures higher than the RST, a local peak can be observed close to the RST. Between the peak temperature and RST, a significant decrease of helix diameter is predicted as the initial pitch increases while the diameters are similar at temperatures higher than the peak temperature.

The investigations of different cross-sectional designs and material arrangements are provided in Fig. 6. The helical microrobots are designed in the investigations with an initial pitch of $100~\mu m$. Fig. 6 a) and b) present the results of shape the deformations with vertical material separation boundaries. The microrobots have either circular or rectangular cross-sections with responsive hydrogel located at the outside of the microrobots. The results show that the data distribution

is similar to the results for the study of different pitches demonstrated before. The microrobot with a rectangular cross-section performed like a microrobot with circular cross-section with an initial pitch less than 100 µm with a decrease in RST. Switching the outside responsive hydrogel to the inside part leads to a dramatic change of the deformation performance. All the cross-sectional designs with responsive hydrogels arranged initially in the inside part of the microrobot studied in this work showed a similar deformation pattern: continuous deformation from the contacted states to regular helical states without a rod state. However, all designs reached a contacted state at around 305K. At temperatures lower than the contacted state temperature, the contact became more compacted as the rapid increase of volume ratio occurs with the lowering of the temperature. For a circular cross-section with an inside responsive material, a fast change



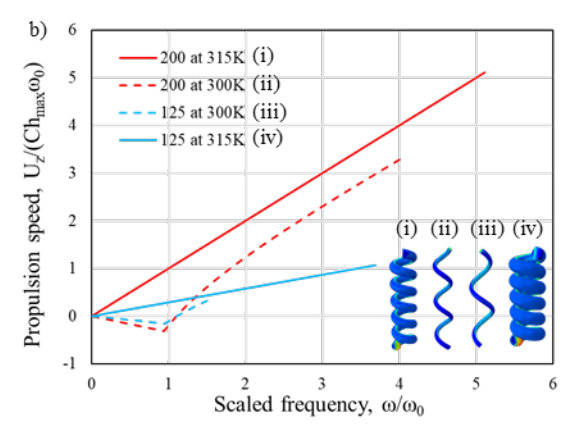


Fig. 7. Dynamics of different microrobots at the non-actuated (300K) and actuated (315K) states. a) Propulsion speed of the half circular and half rectangular cross-sections at different scaled frequencies. b) Propulsion speed of microrobots with different initial helix pitch at different scaled frequencies. The insets are presented with the same order as the legends.

of deformation is found at the initial temperature of 306.6K. The reason for this phenomenon is possibly because the rate of volume change in the temperature range between 306.6K and 307K is the largest across the whole temperature band. This phenomenon is not found in the microrobot with a rectangular cross-section; therefore, this results in a gap in the plot for the helix pitch and turns for these two cross-sections. Overall, these two cross-sections share a similar deformation pattern.

The cross-sectional designs consisting of half circle and rectangle are also investigated as shown in Fig. 6 c) and d). For the material arrangements with vertical separation boundaries, the resulting deformation is similar no matter if the half circle part is on the left (outside) or on the right (inside). The deformations have identical patterns for responsive material in the inside or outside part as discussed.

Material arrangement with horizontal separation boundary is also studied for circular, rectangular, and half circle and rectangle cross-sections. Deformation data for circle cross-section for both vertical and horizontal arrangements with switched location of the responsive material is concluded in Fig. 6 e) and f). From the initial temperature (306.6K), the helix pitch and turns are decreasing and increasing, respectively, whether increasing or decreasing the temperature, forming a more compacted helical microrobot. Deformation is larger as the helix turns increases faster because of the higher

rate of change in volume ratio. No contact state is observed in the studied temperature range. There is identical deformation for the different locations (bottom or top) of the responsive material. This is expected since the change of responsive material from bottom to top is symmetric as the total volumes of the bottom and the top parts are the same. However, this result is also valid for the half circle and rectangular cross-sections.

All the deformations studied in this work preserved their handedness. Therefore, no backward swimming velocity is going to be observed under the same actuation field.

D. Transformation of Dynamics

In this section, some examples of the responsive helical microrobots are studied. Here we use the value $4\pi\chi_0 = 0.1$, which corresponds to a volume fraction of 0.02 with magnetic nanoparticles with a diameter of 11 nm. for the calculation of the magnetic moment described in [22]. In Fig. 7 a), the dynamics of four cases have been investigated for the half circular and rectangular cross-section designs and the arrangement of the materials. As can be seen in the figure, the scaled propulsion speeds at 300K are shown for microrobots with hydrogel material arranged in the inside part of the robot (cases (ii) and (iv)). At 300K both the microrobots present a decent swimming capability while the case (iv) microrobot with the rectangular part on the left side (Outside) shows a better swimming performance with a slightly decreased transition, faster propulsion speed, and larger step-out frequency. At 315K, which is the stimulated state, the filaments of the microrobots are contacted for both cases (ii) and (iv) and thus resulting in zero swimming speed and results not plotted here. Microrobots with hydrogel initially at the outside, cases (i) amd (iii), present an inverse result with 315K (stimulated state) being the temperature where the microrobots are able to swim. However, a reduction of swimming capability can be observed for the outside arrangement (solid lines) compared with the inside arrangement (dashed lines). This is mainly because, for the deformed helical structure, a larger pitch is presented, as can be seen in the inset of Fig. 7 a), and leads to a reduction of the polar angle of the magnetic moment. The presentation of the two branches, forming a circular looking trajectory, of the propulsion speed for the case with rectangular part on the left and hydrogel on the outside part is not abnormal for a helical microrobot with approximately 1 turn for some cases of magnetic moment directions [11].

In Fig. 7 b), the dynamics studies show that the responsive microrobots (with inside hydrogel and circular cross-section) with higher initial pitch have better dynamic performance, both at the non-stimulated and the stimulated states. Microrobots with initial helix pitches of 200 and 125 μm are compared. At the stimulated state (315K), the microrobots transformed to a tighter helical structure with a 90° polar angle Φ , which contributes to the linear increasing of the propulsion speed. For the microrobot with initial pitch of 100 μm , the microrobot reached a contacted state at 315K and thus is not presented here. Therefore, the dynamic performance reduces as the initial pitch reduces. In the meanwhile, the higher pitch at 300K when the initial pitch is 125 μm results in a lower propulsion speed because of the smaller polar angle as discussed above.

Therefore, we can conclude that a vertical arrangement with hydrogel at the outside part has a predominantly better swimming performance. Moreover, a higher initial helix pitch is preferred based on the cases studied in this work. However, if there is a peak performance with higher pitches will be studied in the future work.

IV. CONCLUSION AND FUTURE WORK

In this work, we have studied the shape deformation performance of helical microrobots for adaptive locomotion. The microrobots were assumed to be magnetized through randomly distributed magnetic nanoparticles. Therefore, the isotropic deformation of the hydrogel of the bilayer was investigated for microrobots with different initial helix pitches, cross-sections, and material arrangements. The best shape parameters for adaptive locomotion are further determined through the dynamic modeling of the helical microrobots. Since the deformation of a 3-turn helical microrobot will result in helical shapes with only 1 or 2 turns at some states, a dynamic model that works for arbitrary shapes is used because the helical microrobots at these states do not satisfy the slender body approximation. However, we can conclude that the material arrangements with the responsive hydrogel located in the inside and outside parts can be used for two different situations. First, for helical microrobots with outside located hydrogels, a significant swimming performance can be expected at around room temperature while at the deswelled high temperature regime the helical microrobot will deform to compactly contacted structure without swimming capabilities. Second, a reversed deformation pattern can be used in a switched situation where no swimming capability can be found at low temperature or where a decent swimming capability should be observed at high temperature.

In this model, an assumption of random distribution of nanoparticles was made. However, the magnetic nanoparticles are usually aligned to obtain a pre-defined easy-axis and hence magnetic moment. In this situation, an anisotropic constitutive model of hydrogel should be used and is an area of future work. With the anisotropic model, a planar to helix transformation, typically for structures fabricated by the traditional microfabrication method such as photolithography, can also be simulated. Moreover, the transformation of the magnetic moment should be investigated as a key point.

REFERENCES

- J. C. Breger et al., "Self-Folding Thermo-Magnetically Responsive Soft Microgrippers," ACS Appl. Mater. Interfaces, vol. 7, no. 5, pp. 3398-3405, Feb 11 2015.
- [2] J. Kim, J. A. Hanna, M. Byun, C. D. Santangelo, and R. C. Hayward, "Designing Responsive Buckled Surfaces by Halftone Gel Lithography," *Science*, vol. 335, no. 6073, pp. 1201-1205, Mar 9 2012.
- [3] L. Tan, A.C. Davis, and D.J. Cappelleri, "Smart Polymers for Microscale Machines," Adv. Funct. Mater., p.2007125, Dec 2 2020.
- [4] H. W. Huang, M. S. Sakar, A. J. Petruska, S. Pane, and B. J. Nelson, "Soft micromachines with programmable motility and morphology," *Nat. Commun.*, vol. 7, no. 1, pp. 1-10, Jul 2016.
- [5] J. C. Kuo, H. W. Huang, S. W. Tung, and Y. J. Yang, "A hydrogel-based intravascular microgripper manipulated using magnetic fields," *Sensors and Actuators a-Physical*, vol. 211, pp. 121-130, May 1 2014.
- [6] S. Fusco et al., "An Integrated Microrobotic Platform for On-Demand, Targeted Therapeutic Interventions," *Adv. Mater.*, vol. 26, no. 6, pp. 952-957, Feb 2014.

- [7] H. Zeng, P. Wasylczyk, C. Parmeggiani, D. Martella, M. Burresi, and D. S. Wiersma, "Light-Fueled Microscopic Walkers," *Adv. Mater.*, vol. 27, no. 26, pp. 3883-3887, Jul 8 2015.
- [8] M. Dong et al., "3D-Printed Soft Magnetoelectric Microswimmers for Delivery and Differentiation of Neuron-Like Cells," *Adv. Funct. Mater.*, vol.30, no. 17, pp. 1910323, Apr 2020.
- [9] X. Wang, C. Hu, S. Pane and B. J. Nelson, "Dynamic Modeling of Magnetic Helical Microrobots," in *IEEE Robotics and Automation Letters*
- [10] K. I. Morozov and A. M. Leshansky, "The chiral magnetic nanomotors," *Nanoscale*, vol. 6, no. 3, pp. 1580-1588, Nov 7 2014.
- [11] K. I. Morozov, Y. Mirzae, O. Kenneth, and A. M. Leshansky, "Dynamics of arbitrary shaped propellers driven by a rotating magnetic field," *Phys. Rev. Fluids*, vol. 2, no. 4, pp. 044202, Apr 13 2017.
- [12] ABAQUS, Dassault Systèmes, 2018.
- [13] ABAQUS, User subroutines reference guide. Dassault Systèmes, 2018.
- [14] S. Cai and Z. Suo, "Mechanics and chemical thermodynamics of phase transition in temperature-sensitive hydrogels," *J. Mech. Phys. Solids.*, vol.59, no. 11, pp. 2259-2278, Nov 1 2011.
- [15] P.J. Flory, *Principles of polymer chemistry*. Cornell University Press, 1953
- [16] P.J. Flory, "Thermodynamics of high polymer solutions," J. Chem. Phys., vol.10, no. 1, pp. 51-61, Jan 1942.
- [17] M.L. Huggins, "Solutions of long chain compounds," J. Chem. Phys., vol. 9, no. 5, pp. 440-440, May 1941.
- [18] M.L. Huggins, "Revised theory of high polymer solutions," J. Am. Chem. Soc., vol. 86, no. 17, pp. 3535-3540, Sep 1964.
- [19] W. Hong, X.H. Zhao, J.X. Zhou, and Z.G. Suo, "A theory of coupled diffusion and large deformation in polymeric gels," *J. Mech. Phys. Solids*, vol. 56, no. 5, pp. 1779-1793, May 1 2008.
- [20] H. Mazaheri, M. Baghani, and R. Naghdabadi, "Inhomogeneous and homogeneous swelling behavior of temperature-sensitive poly-(N-isopropylacrylamide) hydrogels," *J. Intel. Mat. Syst. Str.*, vol. 27, no. 3, pp. 324-336, Feb 2016.
- [21] A.V. Filippov, "Drag and Torque on Clusters of N Arbitrary Spheres at Low Reynolds Number," J. Colloid Interface Sci., vol. 229, no. 1, pp. 184-195, Sep 1 2000.
- [22] K. I. Morozov and A. M. Leshansky, "Dynamics and polarization of superparamagnetic chiral nanomotors in a rotating magnetic field," *Nanoscale*, vol. 6, no. 20, pp. 12142-12150, July 25 2014.
- [23] A. M. Leshansky, K. I. Morozov, and B.Y. Rubinstein, "Shape-controlled anisotropy of superparamagnetic micro-/nanohelices," *Nanoscale*, vol. 8, no. 29, pp. 14127-14138, May 19 2016.
- [24] A. F. da Fonseca, C. P. Malta, and D.S. Galvão, "Mechanical properties of amorphous nanosprings," *Nanotechnology*, vol. 17, no. 22, pp. 5620-5626, Oct 26 2006.
- [25] Z. Ding, Z. Liu, J. Hu, S. Swaddiwudhipong, and Z. Yang, "Inhomogeneous large deformation study of temperature-sensitive hydrogel," *Int. J. Solids Struct.*, vol. 50, no. 16-17, pp. 2610-2619, Aug 2013.
- [26] W. Guo, M. Li, and J. Zhou, "Modeling programmable deformation of self-folding all-polymer structures with temperature-sensitive hydrogels," *Smart Mater. Struct.*, vol. 22, no. 11, pp. 115028, Oct 17 2013.
- [27] F. Afroze, E. Nies, H. Berghmans, "Phase transitions in the system poly(N-isopropylacrylamide)/water and swelling behaviour of the corresponding networks," *J. Mol. Struct.*, vol. 554, no. 1, pp. 55-68, Oct 24 2000.